Materials Horizons

ROYAL SOCIETY OF CHEMISTRY

COMMUNICATION

View Article Online
View Journal | View Issue

Cite this: *Mater. Horiz.*, 2022, 9, 1717

Received 14th February 2022,
Accepted 30th March 2022

DOI: 10.1039/d2mh00177b

rsc.li/materials-horizons

Blacklight sintering of ceramics†

Lukas Porz, *[ab] Michael Scherer, [a] Daniel Huhn, [c] Luisa-Marie Heine, [c] Simon Britten, [c] Lars Rebohle, [d] Marcel Neubert, [e] Martin Brown, [f] Peter Lascelles, [f] Ross Kitson, [f] Daniel Rettenwander, [b] Lovro Fulanovic, [a] Enrico Bruder, [a] Patrick Breckner, [a] Daniel Isaia, [a] Till Frömling, [a] Jürgen Rödel [a] and Wolfgang Rheinheimer[ag]

For millennia, ceramics have been densified *via* sintering in a furnace, a time-consuming and energy-intensive process. The need to minimize environmental impact calls for new physical concepts beyond large kilns relying on thermal radiation and insulation. Here, we realize ultrarapid heating with intense blue and UV-light. Thermal management is quantified in experiment and finite element modelling and features a balance between absorbed and radiated energy. With photon energy above the band gap to optimize absorption, bulk ceramics are sintered within seconds and with outstanding efficiency ($\approx$2 kWh kg^{-1}) independent of batch size. Sintering on-the-spot with blacklight as a versatile and widely applicable power source is demonstrated on ceramics needed for energy storage and conversion and in electronic and structural applications foreshadowing economic scalability.

New concepts

Scientists have been enchanted by the search for fast and efficient sintering and explored heating by thermal energy, microwaves and electric fields. The physics behind the energy transfer is intriguing and holds promise for large-scale savings of energy and rapid processing. Particularly, transgressing the intermediate temperature regime, where surface diffusion dominates and squanders driving force for sintering by neck formation, is beneficial for superior microstructural control and processing speed. While conventional furnaces are too slow, electric current with direct attachments of heating elements has demonstrated sintering of ceramics within seconds. Hence, rapid sintering has been proven, but needs to be practical. But how to supply the energy most effectively? Intense illumination! Without the need for a container or contact, it allows rapid heating on-the-spot. Very recent technological availability of high power density at short wavelength allows tuning of incident radiation to the spectral absorption of ceramics boosting both control and efficiency. In consequence, the key to a scalable, fast, efficient and versatile sintering process is optical power transmission with photon energy above the bandgap of ceramics – blacklight.

Introduction

The climate crisis demands a rigid assessment of industrial processes.[1] While 21% of the global green-house emissions stem from industry, 8% of industrial emissions are associated with ceramic industry[2,3] giving a market value of >100 billion $ per year.[4] As firing makes up about 2/3 of the energy need,[3] an increase in energy efficiency of the sintering process dramatically impacts greenhouse gas emission and product price.[5–8] For densifying a ceramic green body, which is driven by a reduction of surface energy,[9] the compacted powder is usually heat-treated for several hours between 1000 °C and 2000 °C in large kilns and furnaces.[10] Such kilns retain radiation and heat and were already constructed by our ancestors for purposes like sintering and burning lime.[11] Nowadays, the required thermal energy is provided *via* thermal radiation and convection from combusting fuel or *via* resistive or inductive heating coils. This entails manifold heat losses by a large heated volume and mass or leaks through the insulation.[12,13] Hence, the energy needed for heating the ceramic itself is surpassed by one to one hundred times by the energy lost in the furnace. While large volumes provide the highest efficiency, they come at considerable cost of flexibility.

Faster, more efficient and more versatile processes of various kinds have been developed and partially established at the laboratory scale. Improved energy efficiency has been demonstrated by avoiding the peak temperature by hydrothermal or cold sintering.[14] Much faster processing times have

[a] *Department of Materials and Earth Sciences, Technical University of Darmstadt, Darmstadt, Germany*
[b] *Department of Materials Science and Engineering, Norwegian University of Science and Technology, Trondheim, Norway. E-mail: lukas.porz@ntnu.no*
[c] *Laserline GmbH, Mühlheim-Kärlich, Germany*
[d] *Institute of Ion Beam Physics and Materials Research, Helmholtz-Zentrum Dresden-Rossendorf, Dresden, Germany*
[e] *Rovak GmbH, Grumbach, Germany*
[f] *Heraeus Noblelight Ltd., Cambridge, UK*
[g] *Institute for Energy and Climate Research, Forschungszentrum Jülich GmbH, Jülich, Germany*

† Electronic supplementary information (ESI) available. See DOI: https://doi.org/10.1039/d2mh00177b

been achieved by establishing a direct contact between the sample and the heating element[6,15] which allows ultrafast heating.[5,16] Processes such as spark plasma sintering[7] or flash sintering,[17,18] however, require electrical contacts and entail electromigration and sometimes electrolytic decomposition. In contrast to direct heating, electromagnetic radiation in the GHz range in microwave sintering allows contact-free heating, however, often low absorption coefficients necessitate susceptors for indirect heat transfer.[19,20] High efficiency at short processing times was recently offered with Xe-flash lamps in the visible light spectrum, however, limited to ultra-short individual flashes to sinter thin surface layers.[21] Outstanding versatility was enabled by using lasers, allowing local heating of areas smaller than 100 μm^2 which enables 3D printing of metals and ceramics.[22] However, scanning point-by-point with a laser instead of heating the whole sample at once, leads to extreme temperature gradients. Moving such a thermal shock zone across the sample invariably prompts microstructural heterogeneity while high density and homogeneity can only be achieved with post processing.

In principle, the potential entailed in fast sintering[5,6] caters to the emerging need in sintering technology for increased flexibility, reduced processing time, and pressingly needed energy efficiency.[1] But the synergy of speed, simplicity, versatility, efficiency, and scalability remained out of striking distance of large-scale production so far.

Herein, we describe a scalable blacklight-based heating process offering container-less and contact-less densification of ceramics within seconds with simple equipment. It utilizes the temperature-dependent absorption of electromagnetic waves in the visible and UV-light frequency spectrum. We demonstrate its speed, versatility and efficiency bundled with intricate microstructural design opportunities using TiO_2 as a model material. Moreover, we demonstrate broad applicability in two dimensions: (i) by testing a wide variety of materials for a range of emerging applications such as batteries, fuel cells, and electro- and structural ceramics in general and (ii) by implementing two completely different light source technologies.

Thermal management

The new process offers a mode of temperature self-stabilization through a balance of absorption of light and emitted thermal radiation of the ceramic itself. Hot bodies, with a light bulb as the prime example, radiate heat as black body radiation. The emitted power density across all wavelengths emitted by an ideal black body E_b is described by the Stefan–Boltzmann law:[23]

$$E_b = \varepsilon\sigma T^4 \quad (1)$$

Aside from the Stefan–Boltzmann constant $\sigma = 5.67 \times 10^{-8}$ W m^{-2} K^{-4}, and the material and temperature dependent emission coefficient ε, E_b only depends on the fourth power of the temperature T. The emitted power density of an ideal black body ($\varepsilon = 1$) in steady-state condition reaches, for example, $\approx$35 W cm^{-2} at 1300 °C.

Absorbed power density can be expressed *via* the incident power density G and absorption coefficient α and equals the black body radiation E_b in a steady state condition. This relation affords self-stabilization at a maximum temperature.

$$\alpha \cdot G = E_b = \varepsilon\sigma T^4 \rightarrow T = \sqrt[4]{\frac{\alpha G}{\varepsilon\sigma}} \quad (2)$$

With thermally insulating substrate, heat exchange with sample support and ambient air turns into a minor, correctable part of the radiation energy balance at very high temperatures. Any additional difference in the absorbed and emitted power density results in a controllable heating or cooling rate.

We demonstrate this process (Fig. 1a) with self-stabilizing temperature (Fig. 1b) and its controllability for samples of 1 mm thickness for several seconds. A ceramic green body is situated on an Al_2O_3/SiO_2 ceramic wool as insulation and illuminated from above with either a pulsed Xe-flash lamp (Fig. 1c) or a 450 nm laser fully illustrated in Fig. 1d–h and Supplementary 1 (Video, ESI†). The temperature during laser illumination with full power applied within $<$1 ms was recorded with a pyrometer as displayed in Fig. 1b documenting a heating rate between 100–500 K s^{-1} and initial cooling with $\approx$200 K s^{-1}. The temperature self-stabilized to $\pm$15 K within 5 seconds (Supplementary 2, ESI†). In contrast, in our approach the entire sample was heated homogenously at once instead of heating voxel by voxel known from selective laser sintering.

Produced samples are contrasted with a conventionally sintered sample (Fig. 1i–k). Microstructure analysis (Fig. 1l–n) demonstrates comparable grain sizes in TiO_2 with densities of $>$94% for the blue (450 nm) laser and $>$98% for the Xe-flash lamp.

Wavelength and absorption

The frequency spectrum of the light source, the absorption characteristics of the material, and its equilibrium with the spectrum emitted by the ceramic are the key parameters for the radiative energy balance. Most oxide ceramics without additives have a bandgap in the range of 2.5 to 5 eV,[24] mostly preventing them from efficiently absorbing, *e.g.*, visible light and long wavelengths. This limits the utility of red and infrared lasers and microwave sintering, where dielectric losses strongly depend on temperature and material.[19,20]

Absorption is maximized if the energy of the incoming photon is larger than the bandgap which can be achieved with blacklight for most ceramics. The wavelength of the available light sources therefore is to be contrasted to the band gap (or absorption edge) to reveal their effectiveness. Fortunately, the effective bandgap reduces by, *e.g.*, 1 eV from room temperature to the sintering temperature.[25–28] Therefore, slightly milder demands are posed onto light sources in the regime where efficiency is needed most allowing also applicability of blue light at high temperatures.

The temperature-dependent spectral absorption is exemplarily highlighted for $SrTiO_3$ single crystals at 22 °C and 1200 °C (Fig. 2a).[26] Even at this high temperature, wavelengths significantly smaller than $\approx$600 nm are needed for effective absorption. Temperature dependent absorption and thermal loss due to infrared emission is highlighted (Fig. 2b) on a $Li_{6.4}La_3Zr_{1.4}Ta_{0.6}O_{12}$

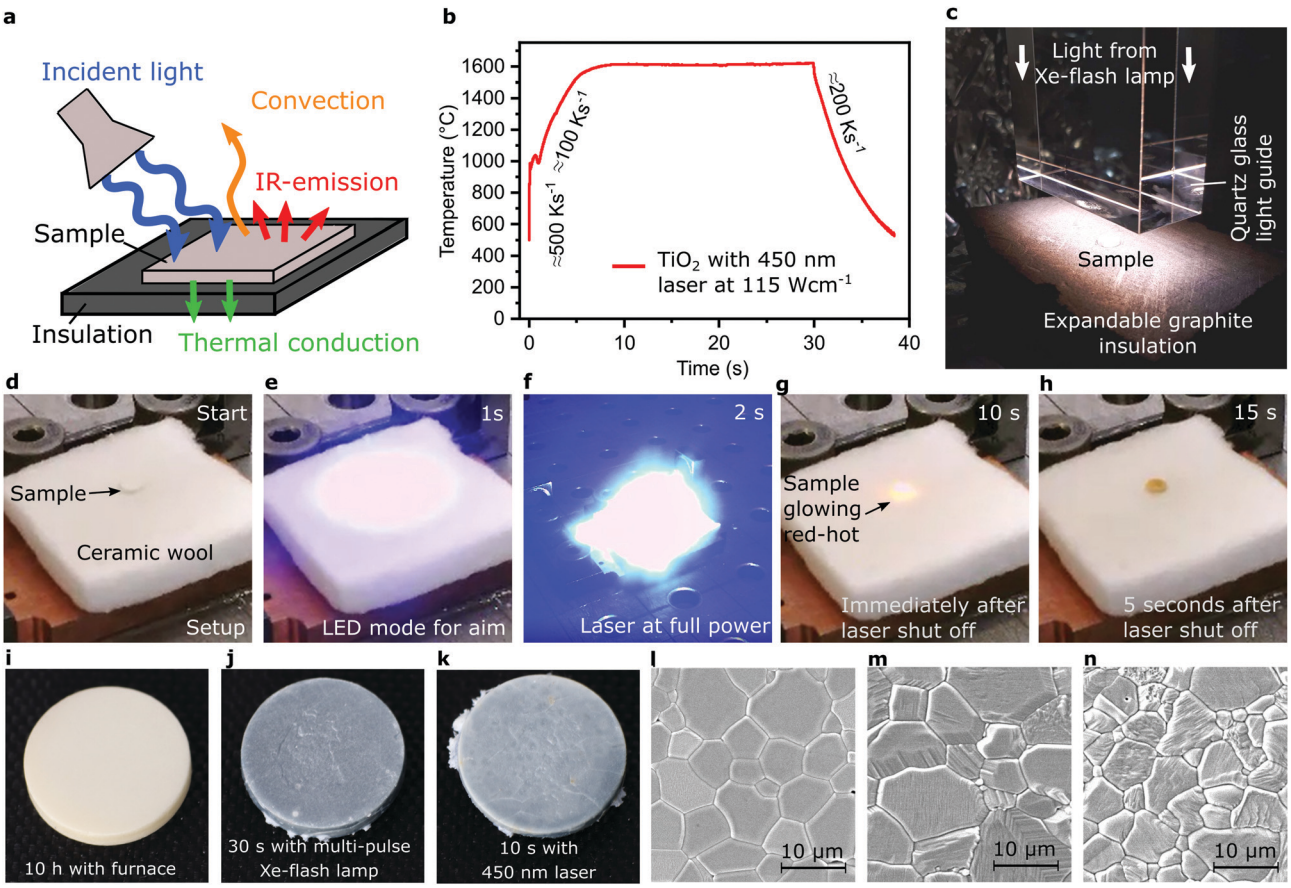

Fig. 1 Concept and experimental implementation of blacklight sintering. (a) Schematic illustrating the key components and four elements of the energy balance. (b) Pyrometer data for temperature during illumination with a blue laser. The discontinuity in temperature during heating is speculated to be due to uneven temperature distribution in the first second of absorption. Verification would require high resolution thermography. (c) Variation of experimental setup with quartz glass guide for the pulsed Xe-flash lamp and a porous expandable graphite sheet as insulation. (d–h) Experimental variation with ceramic wool and illumination with a blue laser, see also Supplementary 1 (Video, ESI†). (i–k), Photographs contrasting sintered pellets between a furnace (i), a Xe-flash lamp (j) and a blue laser (k) (color differences vanish after annealing, *e.g.* at 800 °C). (l–n), Microstructures corresponding to (i–k), respectively.

sample illuminated with 80 W cm^{-2} of 450 nm laser light leading to a sample temperature of about 800 °C. Absorption efficiency rises sharply as the absorption edge moves to lower photon energies due to thermal activation with increasing temperature. This leads to a drastic further temperature increase despite constant illumination associated with a boost in conversion efficiency form $<10\%$ to $>80\%$.

Hence, only with advanced light source technology for high power density at short wavelengths, the prospect of sintering with light unfolds from small volumes to entire bulk parts of ceramics sintered at once. With the recent availability of high-power blue lasers,[29] advanced electronics for Xe-flash lamps and continuing advances in UV-LED-technology letting LEDs approach appreciable power densities as well, a wide implementation becomes imminent.

The insulation beneath the sample is another key factor. This is evidenced by cross sections of two TiO_2 samples illuminated on top of a copper block and on an insulating layer (Fig. 3a and b and Supplementary 3, ESI†) and attendant microstructures (Fig. 3c–e). On a copper block that can divert in the range of 1000 W cm^{-2}, cracking is omnipresent while a large grain size and porosity gradient is observed from top to bottom. When limiting the heat flow into the support to <10 W cm^{-2}, which is then a minor part of the irradiative energy balance, the temperature gradient in the ceramic is minimized (Fig. 3f and g). In consequence, a homogenous microstructure is produced throughout the 1 mm thick sample (Supplementary 4, ESI†).

However, while Al_2O_3/SiO_2 wool or porous board withstands appreciable illumination, its reactivity with many ceramics causes severe issues above certain temperatures (Supplementary 3, ESI†). A counterintuitive solution is to use porous expandable graphite, known from fireproof construction, which erodes during illumination heating. Nevertheless, as process times are below one minute, it withstands the illumination and minimizes reactions with ceramic materials.

Energy efficiency and industrial scaling

The process can become very energy efficient with effective absorption of the incident light and minimized process times.

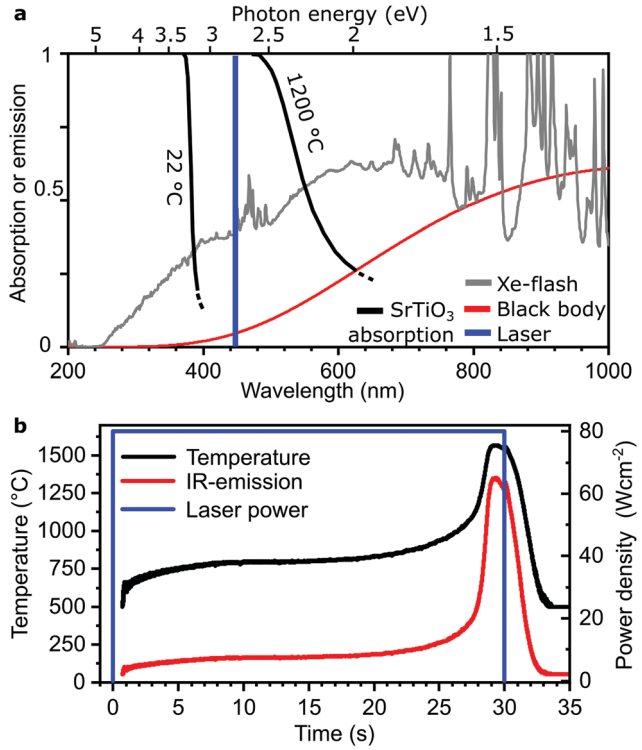

Fig. 2 Effect of wavelength on absorption. (a) Spectral emission of a Xe-flash lamp, an ideal black body at 2700 K, and a blue 450 nm laser overlaid with the temperature-dependent spectral absorption of $SrTiO_3$ single crystals which shifts to lower photon energies (longer wavelengths) with increasing temperature. (b) Temperature evolution under constant illumination of $Li_{6.4}La_3Zr_{1.4}Ta_{0.6}O_{12}$ polycrystalline ceramic with a blue laser highlighting a drastic surge in temperature from a plateau of about 800 °C after absorption efficiency increases with rising temperature.

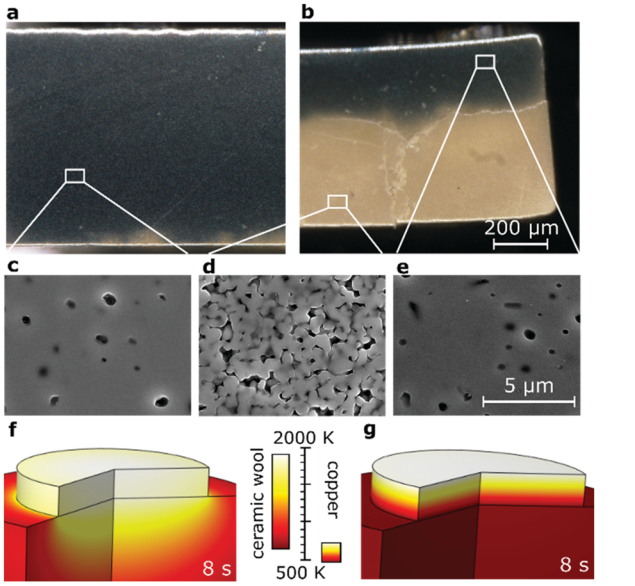

Fig. 3 Illustration of the importance of a thermally insulating sample support. (a) Homogenous sintering result when using insulation. (b) Inhomogeneous sintering outcome with grain size and porosity gradient as well as cracks when using a copper support. (c) SEM image depicting the porosity in (a). (d and e) SEM images revealing the porosity in regions close to the illumination from above and close to the copper block below. (f and g) FEM model of the temperature distribution in (a) and (b) after 8 s illumination illustrating the role of the insulation for a homogeneous temperature distribution in the sample. Temporal evolution can be found in Supplementary 5 and 6 (Video, ESI†).

(All calculations in experimental section.) Merely five seconds were sufficient to successfully obtain dense TiO_2 samples with a 450 nm laser. This required only 0.83 kWh kg^{-1} optical energy input, equaling to 1.88 kWh kg^{-1} electrical input assuming 44% light source efficiency.[29] As already ≈0.36 kWh kg^{-1} are required to heat TiO_2 to 1600 °C, which equals to 43% of the optical energy expended in 5 s illumination, waste heat is kept to a minimum. The Xe-flash lamp's less ideal frequency spectrum leads to the higher energy consumption of ≈4 kWh kg^{-1} (electrical) for comparable fabrication of TiO_2.

A recent comparative study[2] on energy efficiency in sintering using lab-based data highlights cold sintering with 27 kWh kg^{-1} as the most energy-efficient replacement for conventional sintering. Hence, sintering with blacklight with <2 kWh kg^{-1} offers a highly competitive energy efficiency. In comparison, rare publicly available data from industry reports energy needs of, *e.g.*, 13 kWh kg^{-1} for sintering Al_2O_3 in processes mostly based on natural gas.[30]

As no further parameters like external pressure, electrode materials or protective atmosphere need to be considered, production capacity scales almost linearly with illumination power. One 1.5 kW laser can process ≈16 tons per year (1.8 kg h^{-1}), while a 10.5 kW pulsed Xe-flash lamp system can likely process ≈23 tons per year (2.6 kg h^{-1}). Moreover, investments in light sources below 10 000 € per ton annual capacity could be amortized by electricity and CO_2 price savings in less than ten years, see Methods. Lastly, the discontinuous nature of the process allows to adjust production output promptly to the fluctuating availability of renewably produced electricity.

Although efficiency is a strong suit of this technique, the driver for its implementation may be its flexibility and simplicity. In contrast to large-scale kilns, high-efficiency can be achieved independent of batch size using blacklight sintering. Moreover, machinery and parameters can be adapted from individual samples to mass production by merely producing many individual pieces in quick succession. This minimizes the need for development steps in upscaling as parameters and setup can almost be identical at lab scale as well as in mass production. Furthermore, the short process time allows rapid prototyping of new materials, and accessing processing parameters that are very hard to furnish with other methods. Finally, this allows on-demand on-the-spot production of ceramics.

Material design space through temperature control

Lastly, using light as a power medium facilitates agile temperature control with fast heating rates, spatial and temporal evolution opening new possibilities with great versatility. Using only one single high-energy flash from a Xe-flash lamp instead of operating it with quasi-continuous multiple pulses at high

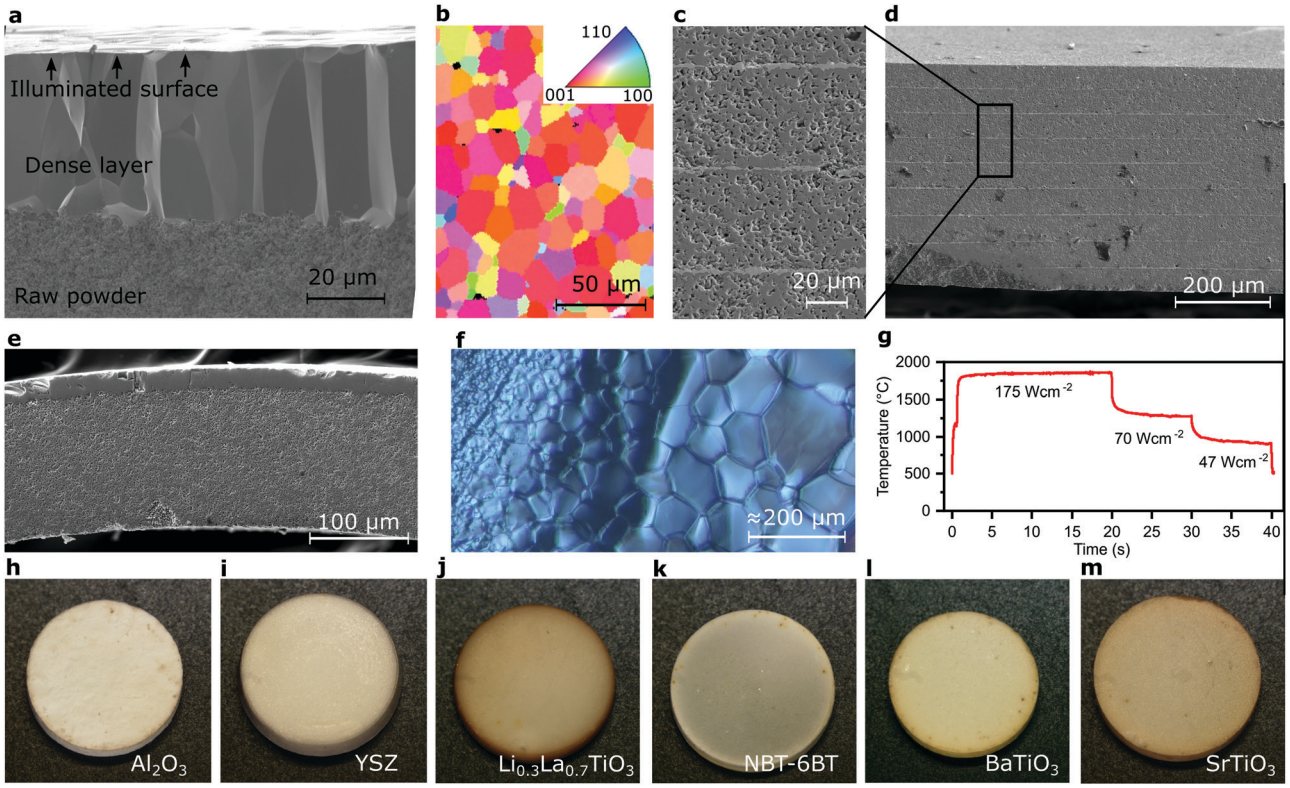

Fig. 4 Illustration of new design space and broad applicability of blacklight sintering. (a) Dense layer formed by single flash from a Xe-flash lamp on pressed TiO_2 powder where grains extend through the entire sintered thickness with completely unsintered raw powder underneath. (b) Electron backscattering diffraction map of the sintered layer. (c) Magnification of (d). (d) Capacitor stack with $BaTiO_3$ layers and Pt electrodes sintered with the 450 nm laser. (e) Sample from (a) after further illumination resulting in a porous but mechanically stable structure underneath. (f) Grain size gradient generated with laser light through varying thermal contact to the support. (h) Illustration of the accuracy of arbitrary temperature profiles. (h–m) photography of six different ceramics sintered with a multi-pulse Xe-flash lamp reaching up to 99.2% density.

frequency allows to selectively heat a thin layer at the surface, *e.g.*, of TiO_2. This layer of about 25 µm thickness is exactly one grain thick (Fig. 4a), with elongated grains with a lateral size of 15 µm. The grains even feature a preferred orientation and, hence, a clear texture (Fig. 4b and Supplementary 7, ESI†) helpful for tailoring materials for catalysis, corrosion, conductivity or anisotropic mechanical properties.

Partially sintering the remainder of the green body with less intense light provides a bi-layer structure from a completely homogeneous green body with a thin dense layer at the top and a porous structure underneath (Fig. 4e). Such design approaches offer immense opportunities for the fabrication of *e.g.* catalytic surfaces, solid oxide fuel cells or gas separation membranes.[31] Similarly, this technique affords sintering two adjacent layers with different temperature profiles or generate lateral grain size gradients or textures (Fig. 4f).

Arbitrary control over the temperature profile (Fig. 4g and 5) also opens new tailoring options. For example, quenched relaxor ferroelectrics offer the option to freeze a high-temperature local structure shifting the depolarization temperature.[32] It can also afford ultrafast sintering without detrimental surface diffusion, which can create dislocations for property modifications[33] or stacking faults.[16] Very rapid sintering also opens the opportunity to minimize evaporation,[6] for example in alkali compounds.[34]

Lastly, this method is demonstrated to be broadly applicable to ceramics. Therefore, a range of ceramics from insulator (Al_2O_3) to oxygen, hole/electron and lithium ion conductor (YSZ, $SrTiO_3$ and $Li_{0.3}La_{0.7}TiO_3$), and ferroelectric $BaTiO_3$ (BT) and $0.94(Na,Bi)TiO_3$–0.06BT (NBT–6BT) were tested. As a rule of thumb, ceramics can be sintered when photon energy exceeds the band gap, which lowers with increasing temperature. While sintering ability is demonstrated, the effect of the higher synthesis temperatures and rates on complex compositions remains to be established. Additives are not required while they may still improve absorption but may hinder phonon transport or cause other side effects. Tested materials also include full electric devices demonstrated for a multilayer capacitor (Fig. 4c and d). Here, BT-multilayers with Pt-electrodes feature excellent homogeneity over the entire thickness of ≈300 µm. All ceramics were cross-validated by using a 450 nm laser and pulsed Xe-flash lamp (Supplementary 8, ESI†). While mechanically sound and crack-free samples were attainable, active control of the heating and cooling ramps (in particular for thicker samples with higher thermal gradient) may lead to further improved integrity and rapid iteration allows to remedy sources of error, such as dust particles or local reaction (Fig. S2b and c, ESI†) quickly. While generally the same outcomes and microstructures could be attained

(Fig. 4 and Supplementary 8–10, ESI†), producing crack-free samples was found to be easier using the Xe-flash lamp as compared to the laser.

Conclusions

Sintering with blacklight enables energy efficiencies down to below 2 kWh kg^{-1} independent of batch size in a container-less and contact-less fabrication process. The choice of photon energy above the bandgap of the ceramic maximizes absorption and allows fabricating homogeneous, textured, or graded ceramic bulk samples of >1 mm thickness with large area. Even complex structures and parts such as multilayer devices can be synthesized within seconds. Unprecedented flexibility needed for on-demand fabrication and rapid development is provided with foreseeable production capacity in the tons-per-year range. Lateral and temporal evolution of the light intensity and, hence, the accurate and rapid control of temperature profiles become powerful tools for microstructural design. Lastly, the rapid densification opens the door to new materials behaviour requiring off-equilibrium synthesis.

Experimental

Synthesis

All green bodies were cold isostatically pressed at 700 MPa with 6.5 mm diameter and approximately 1 mm height except for the samples presented in Fig. 4a–f, which were uniaxially pressed with a height of approximately 200 μm in the case of Fig. 4a, b, e, and f and tape-cast in the case of Fig. 4c and d.

The titanium dioxide reference in Fig. 1i was sintered in a conventional furnace at 1200 °C for 2 h with a heating rate of 5 K min^{-1}.

Illumination was facilitated with three different light sources:

(a) By using a LDMblue 1500 laser with 450 nm wavelength as continuous wave from Laserline (Mühlheim-Kärlich, Germany). The laser was collimated to a spot size of 17 mm. Temperature was tracked using a LPC03 Pyrometer (Mergenthaler, Neu-Ulm, Germany). Illumination experiments were done in the test lab of Laserline.

(b) By using a flexe multi-pulse Xe-flash lamp system from Heraeus Noblelight (Cambridge, UK). The system was operated in multi-pulse mode with a pulse frequency of 60 Hz with 220 V. Average power density was modulated *via* adjusting pulse lengths. Illumination experiments were done in the test lab of Heraeus Noblelight.

(c) Using a Xe-flash lamp array for single flash operations in a flash chamber powered by an energy storage system (300 kJ per pulse at 5 kV in maximum) from Rovak (Grumbach, Germany). Illumination experiments were done in the Helmholtz Innovation blitzlab of the Helmholtz-Zentrum Dresden-Rossendorf.

Illumination parameter and temperatures

Processing parameters for green bodies of ≈1 mm height and 6.5 mm diameter are given below, while representative temperature curves are presented in Fig. 5.

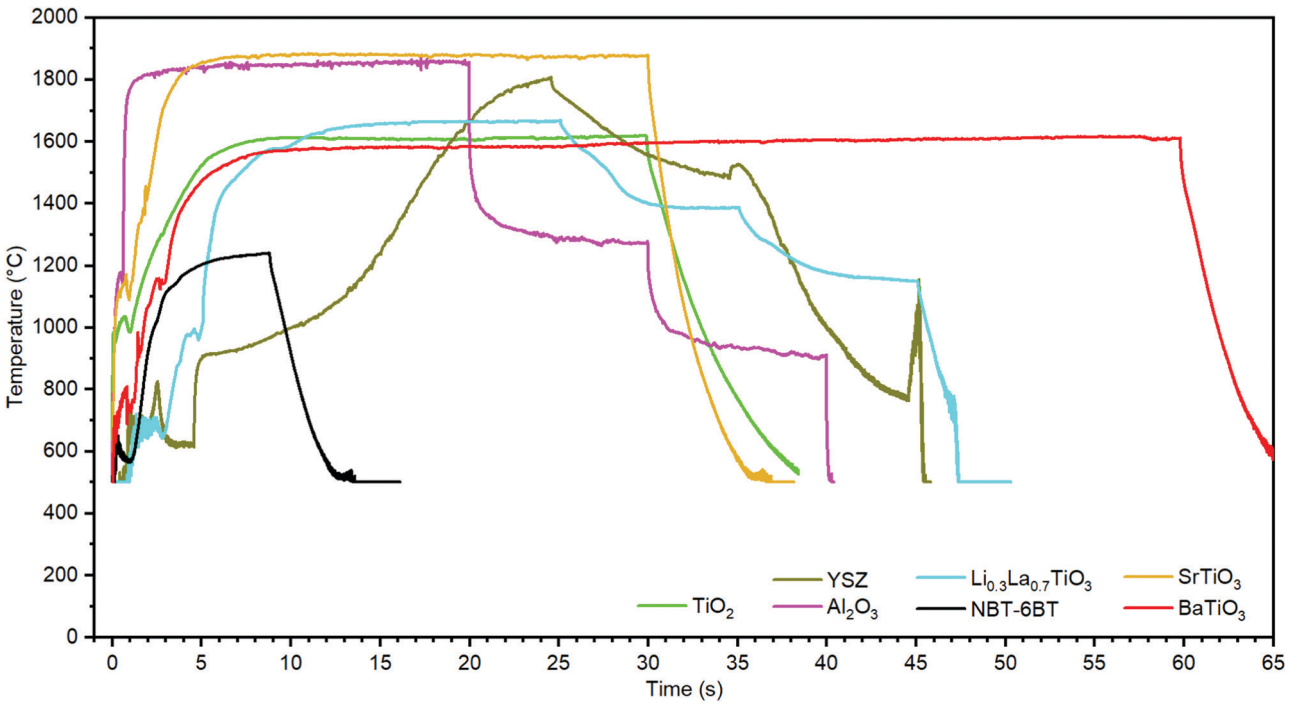

Fig. 5 Temperature data collected with a pyrometer during laser light illumination for different samples. Corresponding illumination parameters, densities and microstructures can be found in Table 1.

Additionally, TiO_2 was sintered with 165 W cm^{-2} of 450 nm laser light with expandable graphite for 5 s reaching a density of 89.7%.

TiO_2 samples in Fig. 3 were processed with 10 s with 135 W cm^{-2} of 450 nm laser light on ceramic wool and 10 s with 150 W cm^{-2} followed by 10 s of 250 W cm^{-2} on a copper block with the same light source.

$BaTiO_3$ multilayer samples containing Pt electrodes in Fig. 4c and d were sintered with the same parameters as specified for $BaTiO_3$ in Table 1. The multilayers were fabricated by tape casting, with detailed description given elsewhere.[35]

A 20 ms pulse with 87 J cm^{-2} produced a fully dense layer on an otherwise unchanged TiO_2 green body (Fig. 4a). The porous structure underneath (Fig. 4e) was generated by further illumination with 10 s of 100 W cm^{-2} 450 nm laser light.

A 200 μm thick TiO_2 green body was illuminated on a copper plate with 200 W cm^{-2} for 10 s resulting in Fig. 4f.

Insulation materials used were expandable graphite GHL (from LUH GmbH, Walluf, Germany) with a density of 90–140 kg m^{-3} and porous Al_2O_3/SiO_2 block (Ultraboard 1850-400P MF from Schupp GmbH, Aachen, Germany) and Al_2O_3/SiO_2 wool (ITM-Fibermax-72 Blanket 1600°/100 from Schupp GmbH, Aachen, Germany with 100 kg m^{-3} density and 12.5 mm thickness).

Spectra and other equipment

Representative spectral data of the Xe-flash lamp was provided by Heraeus Noblelight. The spectral radiance $B_\lambda(T)$ of a black body at 2700 K (a typical temperature for light bulbs) in Fig. 2a was calculated with eqn (3)[23] and normalized to same maximum intensity as the Xe-flash lamp.

$$B_\lambda(T) = \frac{2hc^2}{\lambda^5} \times \frac{1}{\exp\left(\frac{hc}{\lambda k T}\right)} \quad (3)$$

Here, h is the Planck constant, c the speed of light, λ the wave length, k the Boltzmann constant and T the temperature.

The relative density was determined from freshly polished surfaces (down to $\frac{1}{4}$ μm diamond particle size) by assessing the area fraction covered with pores. Representative fractions of the analyzed areas are displayed in Supplementary 9 and 10 (ESI†). In contrast, thermal etching for TiO_2 samples in Fig. 1l–n was done at 1130 °C for 3 hours.

Scanning electron microscopy (SEM) images were acquired using a XL30FEG (Philips, Amsterdam, Netherlands) or a MIRA3-HMX-SEM (TESCAN, Brno, Chech Republic). Electron backscattering imaging and diffraction was done using a MIRA3-HMX-SEM (TESCAN, Brno, Check Republic) equipped with a 4-quadrant solid state BSE detector (DEBEN, Woolpit, UK) and a DigiView V (EDAX, Mahwah, NJ, USA) EBSD detector. All samples were coated with carbon for SEM imaging.

Calculations and approximations

Specific power density needed to keep a constant sample temperature. The green body weight for TiO_2 was 80 mg at 1 mm height and 6.4 mm effective diameter. This results in an

Table 1 Processing parameters and densities

Material	TiO_2	TiO_2	YSZ	Al_2O_3	$Li_{0.3}La_{0.7}TiO_3$	NBT-6BT	$SrTiO_3$	$BaTiO_3$
Insulation	Al_2O_3/SiO_2 wool	Expandable graphite	Expandable graphite	Expandable graphite	Expandable graphite	Expandable graphite	Expandable graphite	Expandable graphite
Laser parameters	135 W cm^{-2}, 10 s	115 W cm^{-2}, 30 s	70 W cm^{-2}, 5 s; 130 W cm^{-2}, 20 s; 70 W cm^{-2}, 10 s; 47 W cm^{-2}, 10 s	175 W cm^{-2}, 20 s; 70 W cm^{-2}, 10 s; 47 W cm^{-2}, 10 s	70 W cm^{-2}, 5 s; 114 W cm^{-2}, 20 s; 70 W cm^{-2}, 10 s; 47 W cm^{-2}, 10 s	67 W cm^{-2}, 10 s	170 W cm^{-2}, 30 s	92 W cm^{-2}, 30 s
Density from SEM images	94.2%	n.a.	86,7%	95.4%	99.2%	95.6%	97.8%	96%
Xe-flash parameters in pulse length and overall duration (always 220 V with 60 Hz)	2 ms, 50 s	1.8 ms, 15 s	2.25 ms, 15 s	2.4 ms, 20 s	1.3 ms, 30 s	1.05 ms, 17 s	2.1 ms, 15 s	1.35 ms, 60 s
Insulation	Al_2O_3/SiO_2 wool	Expandable graphite	Expandable graphite	Expandable graphite	Expandable graphite	Expandable graphite	Expandable graphite	Expandable graphite
Density from SEM images	98.7%	N.A.	87.7%	N.A./too porous	99.3%	81.3%	97.6%	93.8%

illumination area of 0.32 cm^2. The power density needed to maintain a temperature of 1600 °C with a 450 nm laser was 115 W cm^{-2}.

The energy $E_{1600\ °C,1s}$ needed per second (t = 1 s) only to maintain a temperature of 1600 °C can be calculated by the power density j needed to sufficiently illuminate the sample area A divided by the mass m of the sample.

$$E_{1600\,°C,\,1s} = \frac{j \times A}{m} \times t = \frac{115\ \text{W cm}^{-2} \times 0.32\ \text{cm}^2}{80\ \text{mg}} \times 1\ \text{s} = 0.46\ \text{J mg}^{-1} = 0.127\ \text{kW h kg}^{-1} \quad (4)$$

As a result, 0.127 kWh kg^{-1} have to be expended every second to uphold the sample temperature in the current setup.

Energy needed to heat the sample to 1600 °C. Heat capacity of TiO_2 was approximated as independent of temperature with 813 J kg^{-1} K^{-1}.[36] Multiplied with a temperature difference of 1575 K, this amounts to 1.28 MJ kg^{-1} = 0.355 kWh kg^{-1}.

Specific energy needed for the entire process. The sum of the energy E needed for a full illumination process can be determined by multiplying the power density with time and illuminated green body area and dividing it by time.

$$E = \frac{j \times A \times t}{m} \quad (5)$$

Tested parameters using the 450 nm laser:

Energy needed for 150 W cm^{-2} for 5 s: 0.83 kWh kg^{-1} (optical)

Energy needed for 115 W cm^{-2} for 30 s: 3.83 kWh kg^{-1} (optical)

At a conversion efficiency from electrical to optical power of 44% for the blue laser diode,[29] this equals to:

Energy needed for 150 W cm^{-2} for 5 s: 1.88 kWh kg^{-1} (electrical)

The power consumption for a similar sintering process of the multi-pulse Xe-flash lamp was estimated to ≈4 kWh kg^{-1} (electrical).

Production capacity. The production capacity can be estimated by dividing the maximum power output of the light source by the specific energy needed per kg. As products could be moved on a conveyor belt or the light instantaneously be diverted to another area through optics, dead time of the light source can trend to zero in an optimized industrial process.

The production capacity of a blue 1.5 kW laser requiring 3.4 kW electrical input using 1.88 kWh kg^{-1} as specific energy needed is 1.81 kg h^{-1} which equals to 43.5 kg per day or ≈16 tons per year.

The production capacity of a pulsed flash-lamp system operating at 10.5 kW electrical power consumption with a specific energy need of ≈4 kWh kg^{-1} equals 2.62 kg h^{-1} and 63 kg per day or ≈23 tons per year.

Estimation of amortization time. With an approximate investment of less than 10 000 € needed per ton of annual production capacity with off-the-shelf light sources, the amortization time can be estimated with value in energy savings.

For example, a production process needing 10 kWh kg^{-1} of electricity to fire a furnace is replaced by a light-based process needing 3 kWh kg^{-1} of electrical energy.

At an industrial electricity price in Germany of 0.12 € kWh^{-1}, this amounts to a saving of 840 € per ton per year. At average CO_2 emissions of 0.37 kg kWh^{-1} for electricity produced in Germany and a CO_2 price of 50 € per ton, this energy-saving comes along with another 130 € saved on CO_2 emission certificates for 2.6 tons CO_2.

Hence, depending on which process is replaced and many other factors, this technology, has a chance to amortize its needed investments in less than 10 years. This provides an economic incentive to industry to reduce CO_2 emissions and help dealing with the climate crisis.

Model of absorption and evolution of temperature distribution

Accurate modeling would require precise knowledge of light scattering from powder, partially and fully densified ceramics, thermal conductivity as function of density, including composition dependent phonon transport, the dynamic change in roughness and many other parameters which is beyond the scope of this work. In modelling the temperature evolution, nevertheless, the temperature dependent absorption[25,27,28] needs to be taken into account as it is demonstrated to be a key variable in Fig. 2.

Two approaches to calculate the temperature dependent change in light absorption of semiconducting materials are considered. One involves the change of the bandgap due to temperature according to Varshni's rule:[25]

$$E_g = E_{g0} - \gamma \cdot \frac{T^2}{T \cdot \beta} \quad (6)$$

In which E_{g0} is the bandgap at 0 K, T the temperature, and γ and β are constants.

There is, nevertheless, also low light absorption below the energy gap increasing exponentially with the wavelength of light. This is called Urbach tail. The disorder can introduce localized states at the conduction band, which leads to an increase in the band tail width E_U. Thus there is also a proportionality between the absorption coefficient α and E_U:

$$\alpha = \alpha_0 \cdot \exp\left(\frac{h\nu - E_0}{E_U}\right) \quad (7)$$

E_0 is termed Urbach focus and is a measure of the total disorder of the system. α_0 can be seen as a temperature dependent proportionality constant.

The proportionality between E_U and E_g is, however, not easy to determine. Also, the derivation of other parameters can be challenging because γ or β are usually only obtained from calculations that differ significantly from publication to publication. The same is valid for the Urbach focus, especially for oxide ceramics. In the present case, values from a recent publication for TiO_2 are used for a modified relationship of eqn (4):[28]

$$E_g = E_{g0} - \xi \cdot T \quad (8)$$

The further calculation takes the photon energy of the laser of 450 nm into account while the bandgap of E_{g0} = 3.21 eV is used. As a result, a significant rise in absorption can already be observed already at room temperature.

The Urbach approach needs further assumptions obtained from Goldschmidt *et al.*[26] E_U can be assumed to be in the order of kT above room temperature. Furthermore, a proportionality constant σ (in the order of unity) is used so that E_{g0} instead of E_0 can be used leading to the following relationship:

$$\alpha = \alpha_0 \cdot \exp\left(\frac{\sigma(h\nu - E_{g0})}{kT}\right) \quad (9)$$

Additionally, α_0 depends on σ and ξ:

$$\alpha_0 = \alpha_0' \cdot \exp\left(\frac{\sigma\xi}{k}\right) \quad (10)$$

For calculations the proportionality constant is set to σ = 0.8.[28]

The FEM calculation was done for 2D-axial symmetry with the dimensions of the actual samples Fig. 3. For this, the Comsol software (COMSOL Multiphysics, ver. 5.6, Göttingen, Germany) was used. It was assumed that the laser spot was large enough to cover the surface of the sample homogeneously. The respective absorption can be calculated according to:

$$A_{Abs} = 1 - \frac{1}{\log\left(\alpha \cdot \frac{d}{2.303}\right)} \quad (11)$$

In a time-dependent FEM calculation from 0 s to 60 s with 115 W cm^{-2} incident illumination at 450 nm, a triangular mesh was used. The top and side surfaces were cooled by surface to ambient radiation (ambient temperature T_a = 293.15 K) and air convection (heat transfer coefficient h = 50 W m^{-2} K^{-1}). Variations in emissivity ε were also taken into account. It could be shown that ε is linearly dependent on temperature in the high temperature range:[37]

$$\varepsilon = \varepsilon_0 - b \cdot T \quad (12)$$

It was assumed that optimal absorption and emission conditions were still valid at room temperature (ε_0 = 1). A refined model would need to take into account that the samples are not single crystals, however, emission and absorption are likely to be similarly affected by the polycrystalline nature of the specimen. At the bottom, heat transfer to a second material was taken into account. First, ceramic wool and then copper was used as a second material in two different calculations. For the solid itself, literature values for TiO_2 were used (thermal conductivity k = 4.8 W m^{-1} K^{-1}, density ρ = 4.26 g cm^{-3}, heat capacity C_p = 813 J kg^{-1} K^{-1}).[36]

Author contributions

L. P. and W. R. had the key idea. L. P. designed and conceived the study, coordinated collaborations and drafted the manuscript. M. S. and W. R. assisted with experiments and their design. D. H., L.-M. H. and S. B. arranged and facilitated the laser experiments. M. B., P. L. and R. K. arranged and facilitated the multi-pulse Xe-flash lamp experiments. L. R. and M. N. arranged and facilitated the single-pulse Xe-flash lamp experiments. D. R., T. F., J. R. and W. R. assisted with data interpretation and experimental design. T. F. performed FEM simulations. L. F. provided multilayer samples and discussion. E. B. acquired SEM and EBSD images. D. I. and P. B. designed equipment for preliminary experiments. W. R. and J. R. assisted with data interpretation and manuscript writing. All authors have commented on and agreed to the manuscript.

Conflicts of interest

L. P. and W. R. have filed patent applications under number 10 2021 106 117.2 and 10 2021 130 349.4. The involved companies distribute the light source used and may financially benefit from future sales.

Acknowledgements

Sabrina Kahse and Johannes Puy are acknowledged for sample pre- and post-processing. Daniel Bremecker and Florian Flatscher are acknowledged for powder synthesis. The work is supported by project no. 414179371 (J. R.) and RH 146/1-1 (W. R.) of the German Research Foundation (DFG).

Notes and references

1 European Commission, *A policy framewok for climate and energy in the period from 2020 to 2030*, COM/2014/015 final (CELEX:52014DC0015).
2 T. Ibn-Mohammed, C. A. Randall, K. B. Mustapha, J. Guo, J. Walker, S. Berbano, S. C. L. Koh, D. Wang, D. C. Sinclair and I. M. Reaney, *J. Eur. Ceram. Soc.*, 2019, **39**, 5213–5235.
3 E. F. S. Ciacco, J. R. Rocha and A. R. Coutinho, *Appl. Therm. Eng.*, 2017, **113**, 1283–1289.
4 M. Gagliardi, *Am. Ceram. Soc. Bull.*, 2017, **96**, 27–37.
5 M. P. Harmer and R. J. Brook, *Br. Ceram. Trans. J.*, 1981, **80**, 147–148.
6 C. Wang, W. Ping, Q. Bai, H. Cui, R. Hensleigh, R. Wang, A. H. Brozena, Z. Xu, J. Dai, Y. Pei, C. Zheng, G. Pastel, J. Gao, X. Wang, H. Wang, J.-C. Zhao, B. Yang, X. Zheng, J. Luo, Y. Mo, B. Dunn and L. Hu, *Science*, 2020, **368**, 521–526.
7 Z. A. Munir, U. Anselmi-Tamburini and M. Ohyanagi, *J. Mater. Sci.*, 2006, **41**, 763–777.
8 M. Biesuz, T. Saunders, D. Y. Ke, M. J. Reece, C. F. Hu and S. Grasso, *J. Mater. Sci. Technol.*, 2021, **69**, 239–272.
9 R. K. Bordia, S. J. L. Kang and E. A. Olevsky, *J. Am. Ceram. Soc.*, 2017, **100**, 2314–2352.
10 S.-J. Kang, *Sintering: Densification, Grain Growth and Microstructure*, Butterworth-Heinemann, 2004.
11 C. Renfrew and P. Bahn, *Archeology Essentials*, Thames & Hudson, London, 2007.
12 E. Worrell, L. Price, N. Martin, C. Hendriks and L. O. Meida, *Annu. Rev. Energy Environ.*, 2001, **26**, 303–329.

13 H. Jouhara, N. Khordehgah, S. Almahmoud, B. Delpech, A. Chauhan and S. A. Tassou, *Therm. Sci. Eng. Prog.*, 2018, **6**, 268–289.
14 J. Guo, R. Floyd, S. Lowum, J. P. Maria, T. H. de Beauvoir, J. H. Seo and C. A. Randall, *Annu. Rev. Mater. Res.*, 2019, **49**, 275–295.
15 M. Ihrig, T. P. Mishra, W. S. Scheld, G. Häuschen, W. Rheinheimer, M. Bram, M. Finterbusch and O. Guillon, *J. Eur. Ceram. Soc.*, 2021, **41**, 6075–6079.
16 J. Li, J. Cho, J. Ding, H. Charalambous, S. C. Xue, H. Wang, X. L. Phuah, J. Jian, X. J. Wang, C. Ophus, T. Tsakalakos, R. E. Garcia, A. K. Mukherjee, N. Bernstein, C. S. Hellberg, H. Y. Wang and X. H. Zhang, *Sci. Adv.*, 2019, **5**, 5519.
17 R. Raj, *J. Eur. Ceram. Soc.*, 2012, **32**, 2293–2301.
18 M. Cologna, B. Rashkova and R. Raj, *J. Am. Ceram. Soc.*, 2010, **93**, 3556–3559.
19 D. E. Clark, D. C. Folz and J. K. West, *Mat. Sci. Eng. A.*, 2000, **287**, 153–158.
20 A. Thuault, E. Savary, J. Bazin and S. Marinel, *J. Mater. Process. Technol.*, 2014, **214**, 470–476.
21 E. Gilshtein, S. Pfeiffer, M. D. Rossell, J. Sastre, L. Gorjan, R. Erni, A. N. Tiwari, T. Graule and Y. E. Romanyuk, *Sci. Rep.*, 2021, **11**, 3536.
22 A. N. Chen, J. M. Wu, K. Liu, J. Y. Chen, H. Xiao, P. Chen, C. H. Li and Y. S. Shi, *Adv. Appl. Ceram.*, 2018, **117**, 100–117.
23 D. Halliday, R. Resnick and J. Walker, *Fundamentals of Physics, Extended, 10th Edition*, Wiley, 2013.
24 A. Jain, S. P. Ong, G. Hautier, W. Chen, W. D. Richards, S. Dacek, S. Cholia, D. Gunter, D. Skinner, G. Ceder and K. A. Persson, *APL Mater.*, 2013, **1**, 011002.
25 Y. P. Varshni, *Physica*, 1967, **34**, 149–154.
26 D. Goldschmidt and H. L. Tuller, *Phys. Rev. B: Condens. Matter Mater. Phys.*, 1987, **35**, 4360–4364.
27 V. Mishra, M. K. Warshi, A. Sati, A. Kumar, V. Mishra, R. Kumar and P. R. Sagdeo, *SN Appl. Sci.*, 2019, **1**, 241.
28 Y. Cho, A. Yamaguchi, R. Uehara, S. Yasuhara, T. Hoshina and M. Miyauchi, *J. Chem. Phys.*, 2020, **152**, 231101.
29 M. Behringer and H. König, *PhotonicsViews*, 2020, **17**, 60–63.
30 H. Weber, *cfi/Ber. DKG*, 2022, **99**, E17–E20.
31 F. Tietz, Q. Fu, V. A. C. Haanappel, A. Mai, N. H. Menzler and S. Uhlenbruck, *Int. J. Appl. Ceram. Tec.*, 2007, **4**, 436–445.
32 A. Wohninsland, A.-K. Fetzer, A. Riaz, H.-J. Kleebe, J. Rödel and K. V. Lalitha, *Appl. Phys. Lett.*, 2021, **118**, 072903.
33 X. L. Phuah, J. Cho, T. Tsakalakos, A. K. Mukherjee, H. Wang and X. Zhang, *MRS Bull.*, 2021, **45**, 44–51.
34 J.-F. Li, K. Wang, F.-Y. Zhu, L.-Q. Cheng and F.-Z. Yao, *J. Am. Ceram. Soc.*, 2013, **96**, 3677–3696.
35 L. Fulanovic, M. H. Zhang, Y. P. Fu, J. Koruza and J. Rodel, *J. Eur. Ceram. Soc.*, 2021, **41**, 5519–5525.
36 S. J. Smith, R. Stevens, S. F. Liu, G. S. Li, A. Navrotsky, J. Boerio-Goates and B. F. Woodfield, *Am. Mineral.*, 2009, **94**, 236–243.
37 J. M. Jones, P. E. Mason and A. Williams, *J. Energy Inst.*, 2019, **92**, 523–534.

